CONTROL-THEORY AND ADVANCED TECHNOLOGY
Vol.3, No.1, pp.45–72, March, 1987

C87006

Contributed Paper

A FREQUENCY-DOMAIN APPROACH TO FAILURE DETECTION AND ISOLATION WITH APPLICATION TO GE-21 TURBINE ENGINE CONTROL SYSTEMS*

N. VISWANADHAM,[1] J.H. TAYLOR[2] AND E.C. LUCE[3]

Abstract. We present a new design methodology for failure detection and isolation (FDI) and demonstrate its potential for solving the FDI problem in jet engine control systems by applying it to a GE-21 turbofan engine. We first discuss the generalized parity space (GPS) technique for FDI, which is developed in the stable factorization framework. This gives rise to a variety of *parity vector definitions* that are useful for FDI. One result of this approach is that the coefficients of the parity relations necessarily involve stable, proper, rational transfer functions. We also show the equivalence of the parity vector approach with the concept of *failure detection filters*.

We discuss voting schemes for FDI, and the use of Hermite forms and diagonalization as additional aids to failure isolation. By incorporating specific failure models for actuators and sensors, we develop another method for FDI based on the *direction* of the parity vector with respect to certain reference directions defined by the dynamical model. In the same setting, we also develop a simpler method for FDI based on the direction of the *steady-state* parity vector. All of these results represent an extension, simplification and unification of numerous approaches and results for FDI derived via other methodologies.

We demonstrate the potential of this theory by designing an FDI scheme for the GE-21 engine and evaluating it using a nonlinear simulation model of that engine. This study shows that the FDI algorithm is effective and robust, in the sense that most failures can be detected and isolated reliably despite the highly nonlinear nature of the engine dynamics and even when the engine is operating at some distance from the nominal operating point.

Key Words—Failure detection, failure isolation, stable factorization, parity methods, failure detection filters, aircraft engines.

1. Introduction

Our objective is to develop a generalized parity space (GPS) concept based on the stable factorization approach for the detection and isolation of sensor and actuator failures in control systems. This is a critical technology for fault-tolerant control system design; our particular interest is driven by applications to systems such as full-authority digital engine control (FADEC) systems.

Aircraft engines now under development will be built with digital electronic controllers that will increase engine efficiency and performance. However, the

* Received by the editors February 9, 1987.
[1] School of Automation, Indian Institute of Science, Bangalore 560012, India.
[2] Control Technology Branch, GE Corporate R & D, Schenectady, NY 12345, U.S.A.
[3] Systems Research, Kearfott Div., Singer Co., Little Falls, NJ 07424, U.S.A.

use of these sophisticated control laws will make the engine vulnerable to failures of the many sensors, actuators and electronic components used in the control system. Because of this vulnerability, the control system should be fault-tolerant, so that it can perform essential functions under failed conditions. A turbine engine can be made fault-tolerant by installing duplicates of critical components, by providing back-up modes of operation, or by incorporating in the system a reliable means for detecting, isolating and accommodating various malfunctions. We have focussed on the last alternative, by developing the GPS approach and an analytical method for detecting and isolating failures. These results are applied to the FDI problem for the GE-21 jet engine.

1.1 FDI–General background Dynamic failure detection schemes can be thought of as consisting of two stages: *residual generation* and *decision making* based on these residuals (Weiss, Willsky, Pattipati and Eterno, 1985). Outputs from sensors are processed by an appropriate algorithm to generate residual signals which are nominally near zero and which deviate from zero in characteristic ways when particular failures occur. The technique used to generate residuals differs markedly from method to method. In order to be useful in FDI, the residuals must be insensitive to modelling errors, highly sensitive to the particular failures under consideration, quickly responsive when such a failure occurs, and should respond to each failure in an easily-recognized and distinctive manner. In the second stage of decision making the residuals are examined to detect and isolate failures.

Over the past decade, numerous approaches have been developed to solve the problem of fault detection and isolation (FDI) in dynamical systems. The methods include those based on digraphs (Kokawa and Shingai, 1982), fault trees (Teague, 1978), observers (Clark, 1975), Kalman filters (Beattie et al., 1981; Corley and Spang, 1977; Mehra and Peschon, 1971; Willsky and Jones, 1976), parameter identification methods (Isermann, 1984), detection filters (Beard, 1971; Jones, 1973; Meserole, 1981), parity space techniques (Chow and Willsky, 1984; Lou, Willsky and Verghese, 1983; 1986; Potter and Suman, 1977; Weiss, Willsky, Pattipati and Eterno, 1985), etc. See, for example, recent survey articles (Isermann, 1984; Merrill, Lehtinen and Zeller, 1984; Willsky, 1976; 1980) for further background on this topic.

1.2 FDI in the generalized parity space We develop below generalized parity space (GPS) concepts and techniques using the stable factorization (SF) framework. Fault detection and isolation (FDI) using time-domain parity space techniques has been studied extensively. Most work in this area has concentrated on directly redundant systems (Potter and Suman, 1977) where the number of measurements is greater than the number of variables to be sensed. Inconsistency in the measurement data is then a metric that can be used for instrument failure detection. Chow and Willsky (1984) considered parity space generalizations for discrete-time systems using temporal redundancy; they presented an approach for FDI using dynamic parity checks. Lou et al. (1986) consider a frequency domain version of the parity space which is generated as the left null space of the observability matrix of the system. In this case, the parity checks have polynomial coefficients; therefore, to verify the parity check for continuous-time systems, one needs to generate a number of derivatives of the system input and output from the sampled data signals y_k and u_k by using numerical differentiation techniques with the attendant noise problems. In the

discrete-time case, the approach in Lou, Willsky and Verghese (1986) leads to infinite impulse response (FIR) parity checks.

The major contribution below is the development of the GPS based on stable factorizations of the plant model. This ensures that the parity checks have stable, proper, rational transfer functions as coefficients for the input and output measurements; therefore, they can be implemented using stable numerical algorithms in the case of continuous-time systems, and in the discrete-time case, we are not restricted to FIR parity checks with infinite impulse response. The GPS is a more general framework for FDI than the state-space setting (Beard, 1971; Jones, 1973; Meserole, 1981), and unifies the detection filter and parity space approaches that have appeared earlier in the literature cited above. Another advantage is the simplicity of derivation of FDI algorithms using this approach.

1.3 FDI in turbine engines Detection, isolation and accommodation (DIA) of sensor failures in turbine engine control systems has been the subject of several studies in the area, with particular reference to the F-100 engine model. Beattie et al. (1981) formulated five concepts based upon such techniques as Kalman filters; the best one was chosen by conducting tests on digital F-100 engine simulations. A failure-sensitive filter approach was applied by Meserole (1981) to the DIA problem for the F-100 engine; FDI was accomplished by relating the directions of measured residual vectors with a set of known direction vectors associated with various system components. Recently, Weiss, et al. (1985) defined certain FDI metrics and applied them for detection and isolation of sensor failures in turbine engines.

A number of researchers applied DIA techniques to the NASA Quiet, Clean, Short-haul, Efficient Engine (QCSEE). Corley and Spang (1977) studied DIA on the QCSEE under a NASA-sponsored program; this work is referred to as FICA (failure indication and corrective action). The FICA logic detected and isolated failures by simple range checks on the Kalman filter residuals. Merrill, Lehtinen and Zeller (1984) review the various contributions in the area of aircraft turbine engines over the last 10 years.

1.4 Overview In Sec. 2, we survey basic concepts and results from the stable factorization approach that are needed for the development of the FDI methodology. We briefly describe the GE-21 jet engine and present the state-space and stable factorization descriptions of a linearized jet engine model in Sec. 3. Failure models for actuators and sensors are discussed in Sec. 4, and we develop the frequency-domain parity space technique for FDI (the main theoretical result) in Sec. 5. The FDI problem for the GE-21 jet engine is studied in Sec. 6. Simulation results are also presented in this section.

2. Stable factorizations

Before we develop the GPS approach to FDI, it is necessary to outline some of the underlying mathematical framework that provides the basis for the direct formulation of parity vectors and failure detection filter transfer functions (Sec. 5) with the desired properties that they are stable proper rational functions of the Laplace variable s. This framework is central to the stable factorization approach to systems theory (Kailath, 1980; Vidyasagar, 1985).

2.1 The scalar case Consider a scalar transfer function $p(s)$ that is proper and rational. The term *proper* signifies that the numerator degree of $p(s)$ is less than or equal to its denominator degree; *rational* means that $p(s)$ can be expressed in the form of a ratio of polynomials in s. Such a transfer function can always be represented as a ratio of two proper, rational, *stable* functions of s, i.e.,

$$p(s) = \frac{n(s)}{d(s)}, \tag{2.1}$$

where by *stability* we mean that poles lie in the open left half of the complex plane. If we define $\mathcal{S}$ to be the set of all stable proper rational functions, then $n(s)$, $d(s) \in \mathcal{S}$. For example, if $p(s)=(s+1)/(s-1)$, then $n(s)=(s+1)/(s+2)$ and $d(s)=(s-1)/(s+2)$ is one possible pair of stable factors. A rational function $f(s) \in \mathcal{S}$ is said to be a *unit* in $\mathcal{S}$ if and only if it has no zeros in the extended right half plane, i.e., $\{s: \mathrm{Re}\, s \geq 0\}$ including the point at infinity. In other words, $f(s)$ is a unit if and only if both $f(s)$ and $f^{-1}(s)$ are in $\mathcal{S}$; e.g., $f(s)=(s+1)/(s+2)$ is a unit whereas $f(s)=1/(s+1)$ is not.

It is essential to recognize that we are developing factorizations in terms of *stable proper transfer functions* and not polynomials. The importance of this point is primarily in the underlying mathematical theory of this approach; the major practical benefit is that control systems and failure detection algorithms obtained using this machinery automatically have the desirable properties of belonging to $\mathcal{S}$.

Finally, we say that the fractional representation $p(s)=n(s)/d(s)$ is *coprime* if there exist stable proper rational functions $x(s)$ and $y(s)$ such that

$$x(s)n(s) + y(s)d(s) = 1. \tag{2.2}$$

If n and d are polynomials, then (2.2) is equivalent to the requirement that n and d have no common zeros. In our case, where we are dealing with stable proper transfer functions, (2.2) implies that the rational functions n and d have no common zeros in the extended right half plane.

2.2 The matrix case Let $\mathcal{M}(\mathcal{S})$ denote the set of stable transfer function matrices, i.e., matrices whose elements are in $\mathcal{S}$, of whatever order. If the order of the matrix is important, then we will mention this fact explicitly. Also, a matrix U is *unimodular* if $\det U$ is a unit, i.e., $U \in \mathcal{M}(\mathcal{S})$ and $U^{-1} \in \mathcal{M}(\mathcal{S})$.

Given any $n \times m$ proper rational transfer function matrix $P(s)$, we can define the stable right factorization as

$$P(s)=N(s)D(s)^{-1}; \quad N(s) \in \mathcal{M}(\mathcal{S}); \quad D(s) \in \mathcal{M}(\mathcal{S}). \tag{2.3}$$

The matrices $N(s)$ and $D(s)$ can always be found (cf. Sec. 2.3), and are right coprime. This implies that the Bezout identity (the matrix extension of (2.2)) holds:

$$X(s)N(s) + Y(s)D(s) = I, \tag{2.4}$$

where both $X(s)$ and $Y(s)$ are in $\mathcal{M}(\mathcal{S})$. In a similar way, we can define the stable left coprime factorization as

$$P(s)=\tilde{D}^{-1}(s)\tilde{N}(s); \qquad \tilde{D}\in\mathcal{M}(\mathcal{S}), \qquad \tilde{N}\in\mathcal{M}(\mathcal{S}) \tag{2.5}$$

with $\tilde{N}$ and $\tilde{D}$ left coprime. Also, one can find $\tilde{X}(s)$ and $\tilde{Y}(s)$ such that

$$\tilde{X}(s)\tilde{N}(s)+\tilde{Y}(s)\tilde{D}(s)=I, \tag{2.6}$$

where both $\tilde{X}(s)$ and $\tilde{Y}(s)$ are in $\mathcal{M}(\mathcal{S})$. Equating the left and right descriptions (2.3) and (2.5) of $P(s)$, we have the following identity:

$$\tilde{D}N-\tilde{N}D=0. \tag{2.7}$$

In fact, all the identities (2,4), (2.6), (2.7) can be combined to characterize the doubly coprime factorization of $P(s)$ as

$$\begin{bmatrix} Y(s) & X(s) \\ -\tilde{N}(s) & \tilde{D}(s) \end{bmatrix}\begin{bmatrix} D(s) & -\tilde{X}(s) \\ N(s) & \tilde{Y}(s) \end{bmatrix}=\begin{bmatrix} I & 0 \\ 0 & I \end{bmatrix}. \tag{2.8}$$

The two block matrices in the left-hand side of (2.8) are unimodular, and each one is the inverse of the other. Equation (2.8) is called the generalized Bezout identity.

2.3 Stable factors from state-space descriptions It is possible to obtain the left and right stable factors (N,D) and $(\tilde{D},\tilde{N})$ from state-space descriptions of $P(s)$. Suppose we are given a stabilizable, detectable system,

$$\left.\begin{aligned} \dot{x}&=Ax+Bu \\ y&=Cx+Eu \end{aligned}\right\}, \tag{2.9}$$

where A, B, C, E are constant matrices of compatible dimensions. The transfer function matrix of the system is

$$P(s)=C(sI-A)^{-1}B+E. \tag{2.10}$$

Stabilizability and detectability ensure that K and F can be found such that $(A-BK)$ and $(A-FC)$ are stable matrices. Then, we have (Nett, Jacobson and Balas, 1984)

$$\begin{bmatrix} Y & X \\ -\tilde{N} & \tilde{D} \end{bmatrix}=\begin{bmatrix} I & 0 \\ -E & I \end{bmatrix}+\begin{bmatrix} K \\ -C \end{bmatrix}(sI-A+FC)^{-1}\begin{bmatrix}(B-FE) & F\end{bmatrix} \tag{2.11}$$

and

$$\begin{bmatrix} D & -\tilde{X} \\ -N & \tilde{Y} \end{bmatrix}=\begin{bmatrix} I & 0 \\ E & I \end{bmatrix}-\begin{bmatrix} K \\ -(C-EK) \end{bmatrix}(sI-A+BK)^{-1}\begin{bmatrix}B & F\end{bmatrix}. \tag{2.12}$$

We use the above results in our analysis. We refer the reader to Kailath (1980) or Vidyasagar (1985) for further details on the stable factorization approach.

3. Dynamic model of GE-21 jet engine

3.1 Description of the engine The GE-21 engine (see Fig. 3.1) is a double-bypass jet engine with two fans and a two-stage turbine. In a bypass engine, air enters through the inlet which decelerates its flow and increases its temperature and pressure. Then, the main portion of the air bypasses the first fan and a smaller portion goes through the second fan to the compressor. The function of the compressor is to raise the pressure and to reduce the volume of the air as it pumps it through the engine. From the compressor, the air flows to the combustor into which fuel is injected in spray form, mixed with the airstream and ignited. The resultant combustion causes an increase in gas temperature, proportional to the amount of fuel being injected, a moderate increase in velocity, and a small increase in pressure. The high- and low-pressure (HP and LP) turbines provide the shaft power necessary to drive the compressor and rotors by extracting kinetic energy from expanding gases released from the combustor. The extracted energy reduces the temperature and pressure of the gases. The gases from the turbines go through the inner and outer nozzles to

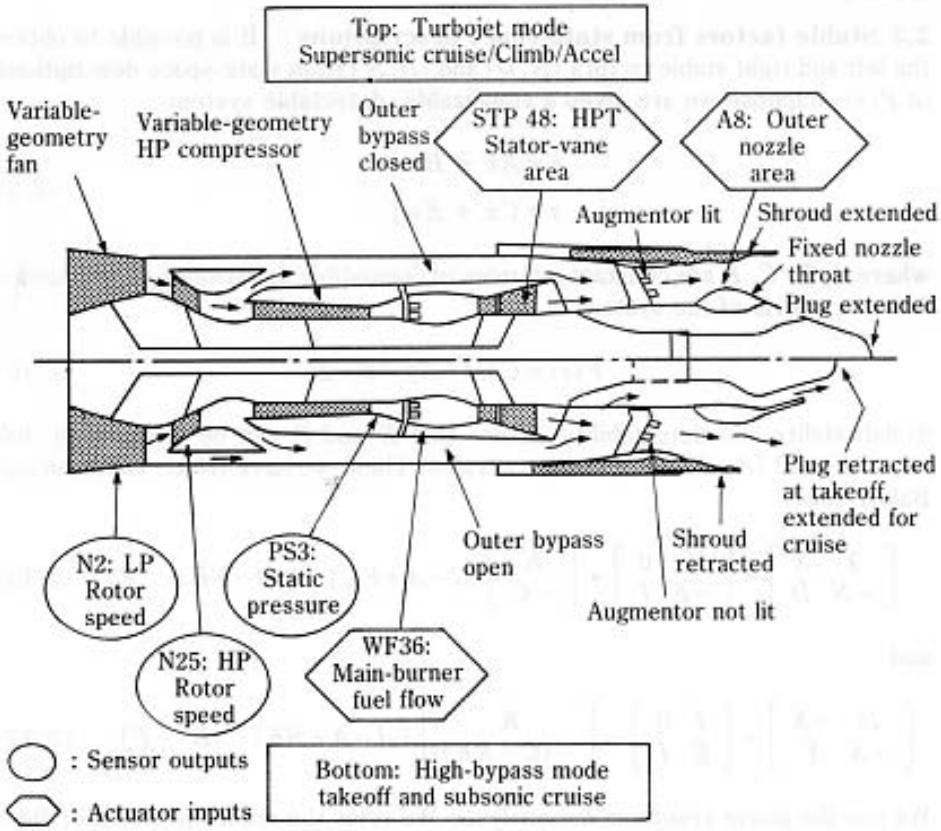

Fig. 3.1. Input and output variables in the GE-21 engine.

the atmosphere. The purpose of full-authority electronic multivariable controllers is to adjust all the control variables of the engine to meet the desired thrust demand without exceeding the physical and thermodynamic limits of the individual components. More information about the GE-21 jet engine is given in Kapasouris (1984) and references therein.

3.2 Nonlinear and linear models The test bed chosen for this study is the nonlinear dynamic simulation model of the GE-21 jet engine (Kapasouris, 1984). This model is capable of simulating the entire operating envelope of the engine. The nonlinear model has two state variables, seven actuators (inputs), and seven sensed or output variables. Three of these input and output variables are primarily used for dynamic feedback control; Table 3.1 presents a list of these variables and the model states. The nonlinear model does not include actuator and sensor dynamics. The actuator servo loops are fast and have output sensors, so we model the actuator dynamics as being instantaneous. These servo loops are isolated, so faults in these mechanisms can be detected and isolated trivially. The sensors used to monitor the engine outputs are also fast enough so that they can be modeled as instantaneous measurements (Kapasouris, 1984).

The nonlinear engine model is approximated by linear models at nine operating points that span the entire engine operating envelope (cruise, takeoff, etc.). Operating point 9, representing takeoff, is selected for the studies presented here. Kapasouris (1984) provides details regarding the values of the variables of interest at each operating point.

To conduct our analysis, we selected the 3-input/3-output linearized model of order 2 corresponding to the variables in Table 3.1. This second-order state-space model at operating point 9 is given by

$$\left.\begin{aligned} \dot{x} &= Ax + Bu \\ y &= Cx + Eu \end{aligned}\right\}, \tag{3.1}$$

Table 3.1. Three-input/three-output GE-21 model variables

	Engine State Variables (x)
N2	LP (Low Pressure) rotor speed [rpm]
N25	HP (High Pressure) rotor speed [rpm]
	Control Inputs (u)
WF36	Main burner fuel flow [lb/h]
STP48	Compressor stator vane [sq in]
A8	Outer nozzle effective area [sq in]
	Outputs (y)
N2	LP rotor speed [rpm]
N25	HP rotor speed [rpm]
PS3	Static pressure at output of the combustor [psi]

where x is a 2×1 state vector, u is a 3×1 input vector, and y is a 3×1 output vector. The numerical values for A, B, C and E are given in Table 3.2.

3.3 Stable factorization description of the engine The state-space model (3.1) of the GE-21 jet engine is given in Table 3.2. We will later make specific use of the following structure for the C and E matrices:

$$C=\begin{bmatrix}1 & 0\\ 0 & 1\\ c_{31} & c_{32}\end{bmatrix};\qquad E=\begin{bmatrix}0 & 0 & 0\\ 0 & 0 & 0\\ e_{31} & e_{32} & e_{33}\end{bmatrix}. \tag{3.2}$$

Next, we use (2.11) to calculate $\bar{D}$, $\bar{N}$. Choose

$$F=[F_1 \quad 0];\quad F_1=A+\sigma I,\quad \sigma>0 \text{ arbitrary} \tag{3.3}$$

With this choice, we note that

$$\bar{N}=\frac{1}{s+\sigma}CB+E, \tag{3.4}$$

$$\bar{D}=I-\left[\frac{1}{(s+\sigma)}C(A+\sigma I) \quad 0\right]. \tag{3.5}$$

Denoting the transfer function matrix of the engine by $P(s)$, we have $P(s)=\bar{D}^{-1}\bar{N}$.

Table 3.2. GE-21 State-space model at operating point 9

$$A=\begin{bmatrix}-3.370 & 1.636\\ -0.325 & -1.896\end{bmatrix}$$

$$B=\begin{bmatrix}0.586 & -1.419 & 1.252\\ 0.410 & 1.118 & 0.139\end{bmatrix}$$

$$C=\begin{bmatrix}1 & 0\\ 0 & 1\\ 0.731 & 0.786\end{bmatrix}$$

$$E=\begin{bmatrix}0 & 0 & 0\\ 0 & 0 & 0\\ 0.267 & -0.025 & -0.146\end{bmatrix}$$

State variables:	N2, N25
Control inputs:	WF36, STP48, A8
Outputs:	N2, N25, PS3

4. Failure models

In the event of failure, the A, B, C, E matrices in (3.1) or $\bar{D}$ and $\bar{N}$ in (3.4) and (3.5) do not represent the jet engine faithfully. Here we specifically consider two general classes of faults: actuator and sensor failures. It is possible to

model the failure of actuators and sensors as additive signals appearing at appropriate places in the model.

4.1 Actuator failures Let u_d be the correct output of the actuators when no failures are present. Let u represent the actual output of the actuator. Then we have

$$u(t) = u_d(t) + a(t), \tag{4.1}$$

where $a(t)$ is a time-varying vector with elements $a_i(t)$. By appropriate choice of $a_i(t)$ we can capture various failure modes of the ith actuator: For example, if the ith actuator freezes at its zero position, producing no output at all, then $a_i(t) = -u_{d_i}(t)$; if there is a bias b_i appearing on the actuator for some reason, then $a_i(t) = b_i$; if the ith actuator is stuck at a constant value k_i, then $a_i(t) = k_i - u_{d_i}(t)$. Multiple failures can be captured in the above setting by specifying several elements of $a(t)$ to be non-zero.

4.2 Sensor failures We model sensor failures in the same way. Let y_d and y represent the sensor desired or true output and the actual output, respectively. Then

$$y(t) = y_d(t) + s(t), \tag{4.2}$$

where $s(t)$ is a time-varying vector with elements $s_i(t)$ representing sensor failures. Complete failure of the ith sensor can be modeled by setting $s_i(t) = -y_{d_i}(t)$, bias failures b_i by setting $s_i(t) = b_i$, and failures where the sensor is stuck at a constant value k_i by setting $s_i(t) = k_i - y_{d_i}(t)$. Again, both single and multiple sensor failures can be modeled using this formulation.

5. The generalized parity space technique

5.1 Derivation of the parity vector relation Consider the linear time-invariant plant depicted in Fig. 5.1, which is described by the $p \times m$ transfer function matrix $P(s)$. Let u_d be the desired or correct control input and u be the actual plant input (output of the actuator); the relation between u and u_d is given in (4.1). Similarly, let y_d be the actual output of the plant (desired or correct sensor output) and y to be the actual output of the sensor; (4.2) expresses the relation between these variables. The variables u_d and y are "external" or available for FDI; u and y_d are "internal" or unaccessible. The relationship among these signals is depicted in Fig. 5.1.

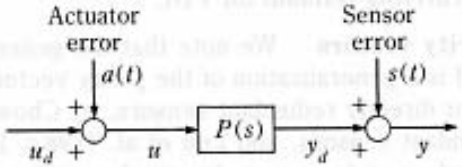

Fig. 5.1. System with sensor and actuator failure models.

In normal operating conditions (no failures), we thus have

$$y(s) = P(s)u_d(s), \tag{5.1}$$

where y and u_d are $p \times 1$ output and $m \times 1$ input vectors respectively. $P(s)$ is the transfer function matrix with right coprime factorization (r.c.f.) (D, N) and left coprime factorization (l.c.f.) $(\bar{D}, \bar{N})$. Also, let z be the partial state of the plant in terms of the r.c.f., in the sense that

$$y = Nz; \quad u_d = Dz. \tag{5.2}$$

We assume that both y and u_d are measured and used in FDI. We thus have access to the extended measurement vector

$$v = \begin{bmatrix} y \\ u_d \end{bmatrix} = \begin{bmatrix} N \\ D \end{bmatrix} z. \tag{5.3}$$

Therefore, by design the range of $\begin{bmatrix} N \\ D \end{bmatrix}$ describes the observation space for FDI. From (2.8) it follows that the matrix $[\bar{D}\ \bar{N}]$ forms the orthogonal complement of $\begin{bmatrix} N \\ D \end{bmatrix}$; thus, we have

$$\bar{D}y - \bar{N}u_d = 0. \tag{5.4}$$

Equation (5.4) can be derived even more directly from (5.1) by noting that $P = \bar{D}^{-1}\bar{N}$. We now define

$$p(s) = \bar{D}y - \bar{N}u_d; \tag{5.5}$$

$p(s)$ is called the *generalized parity vector*, which is defined in the generalized parity space (GPS). We note that $p(s)$ is a p-dimensional vector of rational functions (where p is the number of sensors) and is zero under ideal conditions, i.e., when the plant is linear, noise-free, and there are no failures. Under normal operating conditions, $p(s)$ is a time-varying function of small magnitude due to the presence of noise and modeling errors arising from linearization and order reduction. However, when failures occur, $p(s)$ has a relatively large magnitude representing inconsistencies among the actuator inputs and sensor outputs with respect to the unfailed model. Different failures produce parity vectors with decidedly different characteristics. Thus, the generalized parity vector p may be used as a *signature-carrying residual* for FDI.

5.2 FDI using parity vectors We note that the generalized parity vector we have just defined is a generalization of the parity vectors defined by Potter and Suman (1977) for directly redundant sensors, by Chow and Willsky (1984) for temporally redundant sensors, and Lou et al. (1983; 1986) for polynomial parity checks. Therefore, a frequency-domain description of all parity checks can be very simply and directly based on the l.c.f. of the dynamic plant $P(s)$, as in (5.5). Many of the recently developed approaches to failure detection make implicit or explicit use of the dynamic model as a basis; the above derivation

model the failure of actuators and sensors as additive signals appearing at appropriate places in the model.

4.1 Actuator failures Let u_d be the correct output of the actuators when no failures are present. Let u represent the actual output of the actuator. Then we have

$$u(t) = u_d(t) + a(t), \tag{4.1}$$

where $a(t)$ is a time-varying vector with elements $a_i(t)$. By appropriate choice of $a_i(t)$ we can capture various failure modes of the ith actuator: For example, if the ith actuator freezes at its zero position, producing no output at all, then $a_i(t) = -u_{d_i}(t)$; if there is a bias b_i appearing on the actuator for some reason, then $a_i(t) = b_i$; if the ith actuator is stuck at a constant value k_i, then $a_i(t) = k_i - u_{d_i}(t)$. Multiple failures can be captured in the above setting by specifying several elements of $a(t)$ to be non-zero.

4.2 Sensor failures We model sensor failures in the same way. Let y_d and y represent the sensor desired or true output and the actual output, respectively. Then

$$y(t) = y_d(t) + s(t), \tag{4.2}$$

where $s(t)$ is a time-varying vector with elements $s_i(t)$ representing sensor failures. Complete failure of the ith sensor can be modeled by setting $s_i(t) = -y_{d_i}(t)$, bias failures b_i by setting $s_i(t) = b_i$, and failures where the sensor is stuck at a constant value k_i by setting $s_i(t) = k_i - y_{d_i}(t)$. Again, both single and multiple sensor failures can be modeled using this formulation.

5. The generalized parity space technique

5.1 Derivation of the parity vector relation Consider the linear time-invariant plant depicted in Fig. 5.1, which is described by the $p \times m$ transfer function matrix $P(s)$. Let u_d be the desired or correct control input and u be the actual plant input (output of the actuator); the relation between u and u_d is given in (4.1). Similarly, let y_d be the actual output of the plant (desired or correct sensor output) and y to be the actual output of the sensor; (4.2) expresses the relation between these variables. The variables u_d and y are "external" or available for FDI; u and y_d are "internal" or unaccessible. The relationship among these signals is depicted in Fig. 5.1.

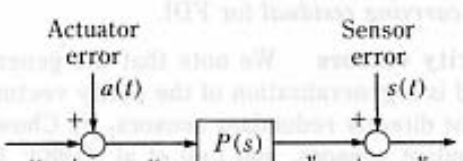

Fig. 5.1. System with sensor and actuator failure models.

unifies all of these disparate results. Finally, the parity vector is essentially equivalent to the output of various failure detection filters described in the literature, as demonstrated in Sec. 5.3.

To illustrate the use of the generalized parity vector, we consider some special cases:

a. Direct redundancy: Suppose there are more measuring instruments than the number of independent variables. Then we can find a constant vector w^T such that $w^T y = 0$, which implies that

$$p_w(s) = [w^T \ 0]\begin{bmatrix} y \\ u_d \end{bmatrix} = [w^T \ 0]\begin{bmatrix} N \\ D \end{bmatrix} z = 0 \tag{5.6}$$

is zero under nominal conditions. This algebraic parity relation is similar to the one in Potter and Suman (1977).

b. Testing a single sensor: Suppose we assume that all actuators are good, i.e., $u = u_d$, and we wish to test the jth sensor. Then, for that sensor, we have

$$y_j = N_j z; \qquad u_d = Dz, \tag{5.7}$$

where N_j denotes the jth row of N. Let $[\lambda_j \ l^T]$ denote the left null space of $\begin{bmatrix} N_j \\ D \end{bmatrix}$ where λ_j is a scalar, l^T is a row vector, and both are members of $\mathcal{M}(\mathcal{S})$. Then, under normal conditions,

$$\bar{p}_j = \lambda_j y_j + l^T u_d = 0. \tag{5.8}$$

When a failure occurs in the jth sensor, the parity variable $\bar{p}_j$ exceeds the threshold and the jth sensor is declared to be faulty.

c. Testing a single actuator: Suppose we assume that all sensors are good and that we want to test the jth actuator. Let D_j denote the jth row of D. Then, under normal conditions, we have

$$y = Nz; \quad u_j = D_j z = u_{d,j}. \tag{5.9}$$

Let $[k^T \ \varkappa_j]$ denote the left null space of $\begin{bmatrix} N \\ D_j \end{bmatrix}$ where $\varkappa_j$ is a scalar, k^T is a row vector, and both are members of $\mathcal{M}(\mathcal{S})$. Then, under normal conditions,

$$\tilde{p}_j = k^T y + \varkappa_j u_{d,j} = 0. \tag{5.10}$$

When the jth actuator fails, $\tilde{p}_j$ exceeds a threshold, thus isolating the faulty actuator.

d. Functional redundancy between two sensors: Let N_i and N_j be the ith and jth rows of N. Then, as in (5.8), we can find l^T, λ_i and λ_j all in $\mathcal{M}(\mathcal{S})$ to obtain

$$p_{ij} = l^T u_d + \lambda_i y_i + \lambda_j y_j. \tag{5.11}$$

We can treat the parity relation (5.11) as a reduced-order model and use it for testing either the ith or jth sensor.

Using similar lines of reasoning, one can derive other parity relations

involving other combinations of sensors and actuators.

5.3 Relations with detection filter methods Failure detection and isolation using detection filters can be interpreted in terms of FDI using the GPV (5.5). Figure 5.2 shows the detection filter configuration in Beard (1971) and Jones (1973). Both Beard (1971) and Jones (1973) choose F such that the error $\bar{e}(t)$ propagates along predetermined constant directions for actuator failures and lies in specific planes for sensor failures. Meserole (1981) applied detection filter methods to be F-100 turbofan engine.

To show the relation of our GPV-based method with the detection filter approach, we first prove that $\bar{e}(s)$ in Fig. 5.2 satisfies the following:

$$\bar{e}(s) = \tilde{D}_y - \tilde{N} u_d, \tag{5.12}$$

where $(\tilde{D}, \tilde{N})$ is the l.c.f. of $P(s)$. To do so, we use (2.11) with $E = 0$: From Fig. 5.2 we have

$$\left.\begin{aligned} \dot{x}_m &= Ax_m + Bu_d + F\bar{e} \\ y_m &= Cx_m \\ \bar{e} &= y - y_m \end{aligned}\right\} \tag{5.13}$$

Laplace transforming (5.13) and eliminating x_m yields

$$\bar{e}(s) = [I - C(sI - A + FC)^{-1}]\, y - [C(sI - A + FC)^{-1}B]u_d. \tag{5.14}$$

Substituting the corresponding relations for $\tilde{N}$ and $\tilde{D}$ ((2.11) with $E=0$) proves that (5.14) is equivalent in form to (5.12). If the matrix F is chosen to stabilize (2.11), then we have shown that the detection filter output $\bar{e}$ is identical with the GPV p in (5.5).

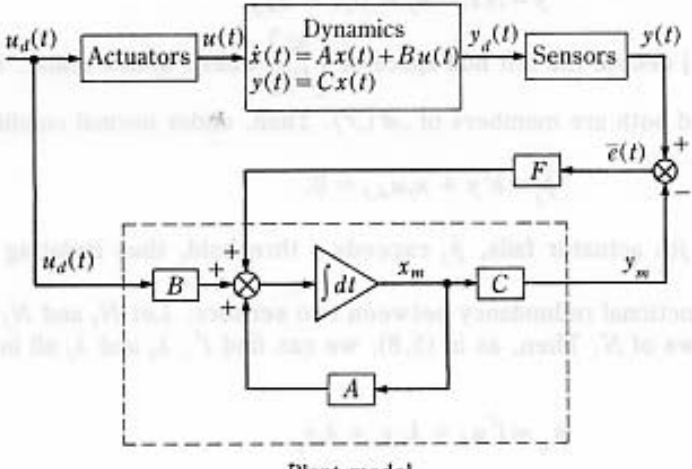

Fig. 5.2. Detection filter configuration.

One advantage of (5.14) is that it provides a state-space realization of (5.5), which may be more readily used for FDI in a digital implementation. Another benefit is that we can directly utilize the methods of Beard (1971), Jones (1973) and Meserole (1981) in the GPS setting—this will be pursued in Sec. 5.4.2.

5.4 Fault isolation in the GPS We consider two ways of using parity relations for fault diagnosis:

a. voting schemes;

and

b. methods using failure directions.

Voting schemes are *more general*, in the sense that no failure model is assumed for components involved, whereas in the method using failure directions we use the sensor and actuator failure models discussed in Sec. 4. The benefit of the latter approach is that isolation can usually be performed unambiguously with a *smaller number of parity variables* than that required using voting. We now proceed to describe the two methods in detail.

5.4.1 General voting schemes To implement a voting scheme with complete isolation for single failures, we need a set of parity relations such that each component, i.e., each actuator and sensor, is involved in at least one parity relation and each component is excluded from at least one parity relation. When a component fails, all the parity relations involving it will be violated, while those excluding it still hold. All the components involved in parity relations that hold are declared to be unfailed, while the component common to all violated parity relations is readily identified as failed.

To illustrate this approach, we consider a three-input/three-output plant. We determine six 3-vectors, namely, $\bar{p}_j; j=1, 2, 3$ using (5.8) and $\bar{p}_j; j=1, 2, 3$ using (5.10). Suppose $\bar{p}_2=\bar{p}_3=0$ and $\bar{p}_1$, $\bar{p}_j; j=1, 2, 3$ are all nonzero. One can then declare y_1 (sensor 1) to be faulty using the above logic. Similarly, if $\bar{p}_1=\bar{p}_2=0$ and $\bar{p}_3$, $\bar{p}_1$, $\bar{p}_2$ and $\bar{p}_3$ are all nonzero, then actuator 3 is faulty.

We can also isolate certain multiple failures using the above six parity relations. Suppose $\bar{p}_2=0$ and $\bar{p}_1$, $\bar{p}_3$, $\bar{p}_j$; $j=1, 2, 3$ are all nonzero. Then the sensors measuring y_1 and y_3 are both faulty. If all of the six parity relations are violated, then at least three components have failed.

The above demonstrates the power of voting schemes for FDI, and also serves to underscore the large number of parity variables that may be involved (18, in this example). This approach can often be simplified by the use of transformations, as the following illustrates:

5.4.1.1 *Voting Schemes Using Hermite Forms*—One can use Hermite forms for $\tilde{D}$ and $\tilde{N}$ plus certain input-output decoupling results to simplify the process of fault isolation. As an illustration, we assume that the actuators are good and demonstrate sensor failure isolation using Hermite forms: Given any l.c.f. $(\tilde{D}, \tilde{N})$, one can always find a unimodular matrix U such that $U\tilde{D}$ is in upper-triangular Hermite from (Vidyasagar, 1985; Kailath, 1980). Premultiplying (5.5) by U (we consider 3 outputs for ease in presentation) yields

$$\begin{bmatrix} \tilde{d}_{11} & 0 & 0 \\ \tilde{d}_{21} & \tilde{d}_{22} & 0 \\ \tilde{d}_{31} & \tilde{d}_{32} & \tilde{d}_{33} \end{bmatrix} \begin{bmatrix} y_1 \\ y_2 \\ y_3 \end{bmatrix} + U\tilde{N}u_d = \begin{bmatrix} p_{v,1} \\ p_{v,1} \\ p_{v,3} \end{bmatrix} = p_v. \qquad (5.15)$$

We can easily arrive at the following conclusions:

a. Only sensor 3 is faulty if $p_{v,1}=p_{v,2}=0$ and $p_{v,3}\neq 0$;

b. Either sensor 2 or sensor 3 or both is faulty if $p_{v,1}=0$ but $p_{v,2}\neq 0$ and $p_{v,3}\neq 0$; and

c. Sensor 1 is certainly failed, and sensor 2 and/or sensor 3 may be failed if all three components are not equal to zero.

Actuator isolation can be done in a similar manner using the Hermite form of $\tilde{N}$ assuming that all the sensors are good. Both of these results are based on the known properties of stable factorizations (Vidyasagar, 1985; Kailath, 1980), and are new with this development.

5.4.1.2 *Voting Schemes With $\tilde{N}$ in Diagonal Form*—Suppose that all sensors are good and that the number of outputs is greater than or equal to the number of control inputs. We can then derive a diagonalized parity vector as follows: Recall from (2.11) (where, for simplicity, we let $E=0$) that

$$\tilde{N}=C(sI-A+FC)^{-1}B, \tag{5.16}$$

where F is any constant nonsingular stabilizing matrix. Now, using the dual results of Viswanadham (1976) and Wolovich (1974) on state feedback decoupling, one can always find J and F such that $J\tilde{N}$ has the following form:

$$J\tilde{N}=\begin{bmatrix} \bar{n}_{11} & 0 & \cdots & 0 \\ 0 & \bar{n}_{22} & \cdots & 0 \\ 0 & 0 & \cdots & \bar{n}_{mm} \\ \cdots & \cdots & \cdots & \cdots \end{bmatrix}. \tag{5.17}$$

If we define a transformed parity vector $\bar{p}$,

$$\bar{p}=J[\tilde{D}_y-\tilde{N}u_d], \tag{5.18}$$

then, using (5.17), we can use the following logic for isolation: If $\bar{p}_j=0$; $j\neq k$, $j=1, 2, \cdots, m$ and $p_k\neq 0$, then the kth actuator is faulty.

5.4.2 Fault isolation using failure directions Another approach to FDI involves using the failure models for sensors and actuators described in Sec. 4 and determining the effect of failures on the parity vector elements. The basic idea is that each failure will result in "activity" of the parity vector along certain axes or in certain subspaces. This information can be used to isolate the fault with fewer parity variables than required using voting based on parity variable magnitude alone; therefore, in many cases this approach is much simpler to implement than a voting scheme. Note that the failure models in Sec. 4 and the failure direction approach were followed by Beard (1971) and Jones (1973) in the state-space setting.

5.4.2.1 *Actuator FDI*—We first consider ith actuator failures modeled by (4.1):

$$u=u_d+a(t);\quad a_i(t)\neq 0;\quad a_j=0,\quad j\neq i. \tag{5.19}$$

Substituting (5.19) into (5.5), and noting that $\tilde{D}_y-\tilde{N}u_d=0$, we get

$$p_{a,i}(s) = -\tilde{N}^i a_i(t), \tag{5.20}$$

where $\tilde{N}^i$ denotes the ith column of $\tilde{N}$. Suppose now that there are at least as many sensors as actuators: Then we can choose F in (2.11) and J such that $J\tilde{N}$ is of the form (5.17). In this instance, (5.20) simplifies to

$$\bar{p}_{a,i}(s) = -\bar{n}_{ii} a_i; \quad p_{a,j} = 0, \quad j \neq i. \tag{5.21}$$

From this relation, we note that no matter what type of failure has occurred (what $a_i(t)$ is), the effect of the ith actuator failure is always characterized by activity along the ith axis in the GPS; thus, we refer to the first m axes (where m is the number of actuators) in the coordinate frame of $\bar{p}(s)$ under (5.17) as the *actuator failure direction set* in the parity space.

5.4.2.2 *Sensor FDI*—Suppose the ith sensor has failed as modeled in (4.2). Following the same procedure as above, we obtain

$$p_{s,i}(s) = \tilde{D}^i s_i(t), \tag{5.22}$$

where $\tilde{D}^i$ denotes the ith column of $\tilde{D}$. The domain of the activity of the parity vector under the assumption that the ith sensor has failed depends on the number of non-zero elements in $\tilde{D}^i$. Unfortunately, it is not possible, in general, to choose F and J such that $J\tilde{D}$ is diagonal as in the case $\tilde{N}$. However, the parity vector always lies in a plane or higher-dimensional subspace of the GPS; this information can still be used for sensor FDI by projecting the parity vector onto the appropriate subspaces as demonstrated in Sec. 6 in our application to the GE-21 engine. In particular, we show that considering the *steady-state* parity vector subspace leads to a simple and effective sensor FDI scheme.

6. Application to the GE-21 engine

We now apply the generalized parity space (GPS) approach developed in Sec. 5 to formulate two failure detection and isolation algorithms for the GE-21 engine. A single *failure detection filter* will be designed using the stable factorization approach to generate the generalized parity vector, and *detection* will be carried out by monitoring the magnitude of the parity vector. *Isolation* will be based on parity vector direction in the GPS: In both algorithms, actuator fault isolation will be accomplished by the *steady-state GPV direction method*; sensor failure isolation will be carried out using the steady-state GPV direction method for the bias error case and by the *GPV subspace projection method* when the errors are time-varying. These approaches are based on the developments provided in Sec. 5.4.2.

The general description and stable factorization model of the GE-21 jet engine were given in Sec. 3. In particular, we consider the three-input/three-output jet engine model given in (3.1), (3.2), and Table 3.2. The FDI scheme has to detect and identify failures in 6 components: 3 actuators and 3 sensors. The three sensors measure the variables N2 (LP rotor speed), N25 (HP rotor speed), and PS3 (compressor discharge pressure); the three actuator servo outputs are WF36 (fuel flow), STP48 (LP turbine stator position), and A8 (outer nozzle area). As mentioned previously, the actuator servo loops and sensors are

assumed to be instantaneous in this study.

6.1 Generalized parity relation for the GE-21 engine In the development that follows, we use the parity Eq. (5.5) with a slight extension, i.e.,

$$p(s) = J(s)[\bar{D}(s)y(s) - \bar{N}(s)u_d(s)], \tag{6.1}$$

where $J(s)$ is any stable, rational, proper matrix of transfer functions ($J(s) \in \mathcal{M}(\mathcal{S})$) yet to be chosen. This matrix is introduced simply to add another "degree of freedom" so that the parity vector form can be simplified. Recall that $y(s)$ represents sensor outputs, and $u_d(s)$ denotes the outputs of the actuator position and fuel flow servo-loop sensors. Also, $(\bar{D}\ \bar{N})$ is the l.c.f. of the engine without actuator and sensor dynamics (see Sec. 3) and is given by

$$\bar{N} = \frac{1}{s+\sigma} CB + E, \tag{3.4}$$

$$\bar{D} = I - \left[\frac{1}{(s+\sigma)} C(A+\sigma I) \quad 0\right]. \tag{3.5}$$

Our aim is to determine $J(s)$ and σ such that generalized parity vector (GPV) $p(s)$ is small under nominal conditions and large when failures are present, $p(s)$ responds rapidly to failures, and so that each of the six failures should produce characteristically different parity residuals, thus providing clear isolation.

Let T be an arbitrary 3×3 nonsingular constant matrix and C_3, E_3 denote the third rows of C and E (see (3.2)), and define

$$\left.\begin{aligned} J(s) &= T\begin{bmatrix} I_{2\times2} & 0 \\ \dfrac{1}{s+\sigma}C_3 & \dfrac{1}{s+\sigma} \end{bmatrix}; \qquad B_n = T\begin{bmatrix} B \\ E_3 \end{bmatrix} \\ E_d &= T\begin{bmatrix} I_{2\times2} & 0 \\ 0 & 0 \end{bmatrix}; \qquad B_d = T\begin{bmatrix} -(\sigma I + A) & 0 \\ -C_3 & 1 \end{bmatrix} \end{aligned}\right\}. \tag{6.2}$$

The expression for J was determined by considering the structure of the GE-21 state-space model (3.2) and attempting to achieve as much simplicity as possible; the remaining definitions are made to simplify the formulation of the GPV. Premultiplying (3.4) and (3.5) by $J(s)$ and using (6.2), we obtain

$$J\bar{N} = (s+\sigma)^{-1}B_n, \tag{6.3}$$

$$J\bar{D} = E_d + (s+\sigma)^{-1}B_d. \tag{6.4}$$

Using (6.3) and (6.4) and the generalized parity Eq. (6.1), we can derive the GPV for various sensor and actuator failures:

a. Suppose a failure of type (4.1) occurs in the ith actuator. Then the GPV generated due to this failure is given by

$$p_{a,i}(s) = -B_n{}^i \frac{a_i(s)}{(s+\sigma)}, \tag{6.5}$$

where $B_n{}^i$ denotes ith column of B_n and $a_i(s)$ denotes the scalar Laplace

transform of the error signal $a_i(t)$. The form of (6.5) is a constant vector $B_n{}^i$ times a scalar function of s; therefore, it is clear that $p_{a,i}(s)$ is confined to exhibit activity along the direction defined by the vector $B_n{}^i$ in the GPS. Thus, if the monitoring system determines that the parity vector is large and nearly co-linear with the vector $B_n{}^i$, then a failure in the ith actuator is declared.

b. Now we consider sensor failures of the type modeled by (4.2). Equation (6.4) shows that sensor failures result in a parity vector of the form,

$$p_{s,i}(s) = \left[E_d{}^i + \frac{B_d{}^i}{(s+\sigma)} \right] s_i(s), \tag{6.6}$$

where $B_d{}^i$ and $E_d{}^i$ denote the ith columns of B_d and E_d respectively, and $s_i(s)$ denotes the scalar Laplace transform of the sensor error signal $s_i(t)$. Equation (6.6) shows that:

i. For failures in sensors 1 and 2, the parity vector $p_{s,i}(s)$ lies in a plane. A failure of the first sensor generates a GPV $p_{s,1}(s)$ which is constrained to lie in the plane defined by the vectors $[t_{11}\ t_{21}\ 0]^T$ and $B_d{}^1$, and a failure of the second sensor generates $p_{s,2}$ in the plane formed by $[t_{21}\ t_{22}\ 0]^T$ and $B_d{}^2$. If the parity vector is observed to lie primarily in one of these planes, then the corresponding sensor failure is indicated.

ii. For a failure in sensor 3 of the type (4.2), the parity vector is given by

$$p_{s,3}(s) = B_d{}^3 \left(\frac{s_3}{s+\sigma} \right), \tag{6.7}$$

which is obtained by substituting (4.3), (6.3) and (6.4) into (6.1). From (6.7), it is clear that the appearance of a parity vector of substantial magnitude aligned with the vector $B_d{}^3$ is indicative of PS3 sensor failure.

It is not difficult to determine the plane of activity for the GPV under sensor 1 or 2 failure and isolate faults based on that information, as we will demonstrate in Sec. 6.3.2. However, if the failure is of the bias type, it is easier to use the steady-state behavior of the GPV for fault isolation.

6.2 Isolation using the steady-state GPV Suppose failures in the above components are of the step or bias type. Since $J(s)$, $N(s)$ and $D(s)$ are all stable matrices, we can use the final value theorem to compute p^{ss}, the steady-state parity vector. Failure identification can be accomplished based on the direction in which the steady-state GPV exhibits activity:

a. Suppose a constant bias of magnitude b_i develops on the ith actuator sensor. Then taking the limit of $[s\, p_{a,i}(s)]$ (6.5) as $s \to 0$ with $a_i(s) = b_i/s$, we get

$$p_{a,i}{}^{ss}(s) = -B_n{}^i \frac{b_i}{\sigma}; \tag{6.8}$$

b. If a constant bias of magnitude c_i develops on ith sensor, then applying the same procedure to (6.6) yields

$$p_{s,i}{}^{ss} = B_s{}^i \frac{c_i}{\sigma}, \tag{6.9}$$

where

$$B_s = (\sigma E_d + E_d).$$

From (6.8) and (6.9), it is clear that the steady-state GPVs p_a^{ss} and p_s^{ss} lie in fixed directions for all six failures under consideration. The directions along which the GPV appears are defined by the three columns of B_n and the three columns of the matrix B_s. We choose the constant matrix T in (6.2) so these directions are well separated and thus isolation is easy. For a choice of $\sigma=5$ (for fast response; this is roughly twice the magnitude of the eigenvalues of A, i.e., $\lambda(A)=-2.74,\ -2.53$) and

$$T=\begin{bmatrix} 0.245 & 1.255 & -0.738 \\ 0.914 & 0.744 & 2.180 \\ -0.167 & 0.124 & -3.357 \end{bmatrix}, \tag{6.10}$$

the angles between the column vectors of B_n and (σE_d+B_d) are calculated and given in Table 6.1. From this table, it can be seen that the reference failure directions exhibit good separation.

To mechanize this algorithm, we set up the transfer functions $J\bar{N}$ and $J\bar{D}$ according to (3.4), (3.5), (6.2), and (6.10) to generate the generalized parity vector (6.1). This vector magnitude is monitored, and a failure is declared whenever it becomes large compared with the nominal value. In addition, we incorporate logic to determine when the GPV has achieved steady state, and implement a projection algorithm to find the angle between each of the reference directions (columns of B_n and B_s) and the GPV direction. Failure is then associated with that sensor or actuator whose reference direction is closest to the GPV.

Table 6.1. Analytic steady-state angles between GPV and reference directions (transformed system)

2nd reference direction	1st reference direction (angles in degrees)					
	Actuator			Sensor		
	WF36	STP48	A8	N2	N25	PS3
WF36	0	75	53	82	55	28
STP48	75	0	78	88	28	59
A8	53	78	0	30	80	75
N2	82	88	30	0	75	75
N25	55	28	80	75	0	32
PS3	28	59	75	75	32	0

6.3 Simulation results In all of the studies presented in this section, we induce failures in the nonlinear simulation model that correspond to sensor or actuator faults as defined in Sec. 4 ((4.1), (4.2)). In all cases, the actual input signals to the engine actuator loops were constant and the engine initial conditions were chosen to correspond to steady state; therefore, if there is no fault, the state variables and sensor outputs are also constant.

The errors introduced in the actuator or sensor signals were of two types:

- The "standard" fault was a bias error that ramped up to a steady-state value

over a one-second interval. The steady-state value is determined by taking a fixed percentage of the nominal (unfailed) value. In one case, a longer ramp time (20 [sec.]) was chosen so that an actuator nonlinear effect could be examined. These studies provided the basis for demonstrating the capabilities of the FDI algorithm based on steady-state GPV direction.

- The second fault considered was the injection of a sinusoidal error signal having a period (2 [sec.]) that is considerably longer than the time constants of the engine (about 0.4 [sec.]). This allowed us to show that the steady-state GPV method is able to isolate non-bias actuator faults, and that projecting the GPV onto the appropriate subspace achieves good sensor FDI, at a modest cost in terms of added complexity compared with the GPV steady-state algorithm.

These error models were used to generate measurement and input data to test the FDI algorithm presented in Sec. 6.2.

6.3.1 Bias error results Tables 6.2 and 6.3 display the GPV magnitude and steady-state angles between the GPV and the failure reference directions for

Table 6.2. Steady-state angles between GPV and reference directions (transformed system, −5[%] ramp failure)

Failure	GPV/reference directions (angles in degrees)						GPV magnitude
	Actuator			Sensor			
	WF36	STP48	A8	N2	N25	PS3	
NO FAILURE	34.5	56.5	80.3	69.4	29.1	6.2	2.7E-05
WF36	0.4	75.4	52.3	81.7	55.0	28.7	1.3E-02
STP48	74.5	0.8	77.1	88.3	27.6	58.8	1.4E-02
A8	89.2	73.4	42.9	15.1	59.6	63.0	6.3E-03
N2	82.0	87.6	30.5	0.1	74.7	74.5	2.3E-02
N25	54.6	27.6	80.5	74.7	0.0	32.5	4.0E-02
PS3	28.3	59.0	75.0	74.6	32.5	0.0	2.9E-02

Table 6.3. Steady-state angles between GPV and reference directions (transformed system, −10[%] ramp failure)

Failure	GPV/reference directions (angles in degrees)						GPV magnitude
	Actuator			Sensor			
	WF36	STP48	A8	N2	N25	PS3	
NO FAILURE	34.5	56.5	80.3	69.4	29.1	6.2	2.7E-05
WF36	0.8	75.7	52.1	81.5	55.4	29.1	2.7E-02
STP48	75.7	1.9	77.0	89.2	29.2	60.4	2.7E-02
A8	71.0	61.8	62.8	33.8	42.2	43.7	1.4E-02
N2	82.0	87.6	30.5	0.0	74.7	74.6	4.7E-02
N25	54.6	27.6	80.5	74.7	0.0	32.5	7.9E-02
PS3	28.3	59.0	75.0	74.6	32.5	0.0	5.8E-02

errors of −5[%] and −10[%] of per unit value in each of the six components, respectively. The failure actually takes 1 second to settle to the steady-state value of −5[%] or −10[%] so that transient effects of the fault can be observed; for example, see Fig. 6.1. First, we discuss the results presented in Table 6.3; those in Table 6.2 can be interpreted similarly. Then we will consider Fig. 6.1 in detail.

When there is no failure, the GPV magnitude is of the order of 10^{-5}. For a −10[%] bias in any of the components, the GPV magnitude increases by approximately a factor of 10^3, and −5[%] biases resulted in a minimum GPV magnitude increase by a factor of 233. Failure detection is thus assured, even for small errors.

Next, we examine the isolation capabilities of the steady-state algorithm: Consider actuator 1 failure: for a −10[%] bias in WF36, the angle between the parity vector and the column vector B_n^1 is 0.8°, whereas the vectors B_n^2, B_n^3, B_s^1, B_s^2, B_s^3 are all well separated from the direction of the parity vector. (The minimum separation in these five directions is 29.1°.) Thus, a steady-state GPV along B_n^1 is clearly indicative of actuator 1 failure. Similarly, in the cases where there is a −10[%] bias in STP48, N2, N25, or PS3, such a failure is definitively indicated by the parity vector residual being aligned with B_n^2, B_s^1, B_s^1, or B_s^3, respectively. Disregarding the remaining actuator (A8) for a moment, we note that the maximum "diagonal" GPV/failure reference direction angle is 1.9° while the minimum "off-diagonal" angle is 27.6°; this indicates excellent isolation for the five faults discussed so far.

Before dealing with the question of fault isolation for A8, we will present time histories for the actuator 1 fault. The first panel of Fig. 6.1 shows the −10[%] error building up in the WF36 (actuator or input 1) signal, and the panel below shows the corresponding GPV magnitude increase. The upper right panel shows that the angle between the GPV and the reference direction for actuator 1 very rapidly drops to near zero, while the remaining five angles between the GPV and other reference directions quickly settle to large values. Thus, we achieve both clear and rapid isolation of the fault based on the steady-state GPV direction. (Observe that the six angle signals have arbitrary values before the fault takes place, and thus they should be ignored until the GPV magnitude exceeds a threshold value.)

Table 6.4. GPV/failure reference direction angles, bias errors in Actuator 3 (A8)

A8 [%] bias	$p_{a,3}^{ss}/B_n^3$ Angle
−10	63°
−5	43°
−2	13°
−1	8°

Tables 6.2 and 6.3 show that failures in the A8 actuator servo sensor are readily detected but not so clearly isolated. To investigate this problem more fully, we simulated smaller bias errors (−1% and −2%) and found that the isolation becomes less ambiguous as the error decreases in magnitude. The respective angle magnitudes between the GPV and the A8 failure reference direction are indicated in Table 6.4. Clearly, as the error becomes smaller, the FDI algorithm is "converging"; we thus attribute the poor behavior for −5[%] and −10[%] bias errors to the highly nonlinear nature of the GE-21 engine.

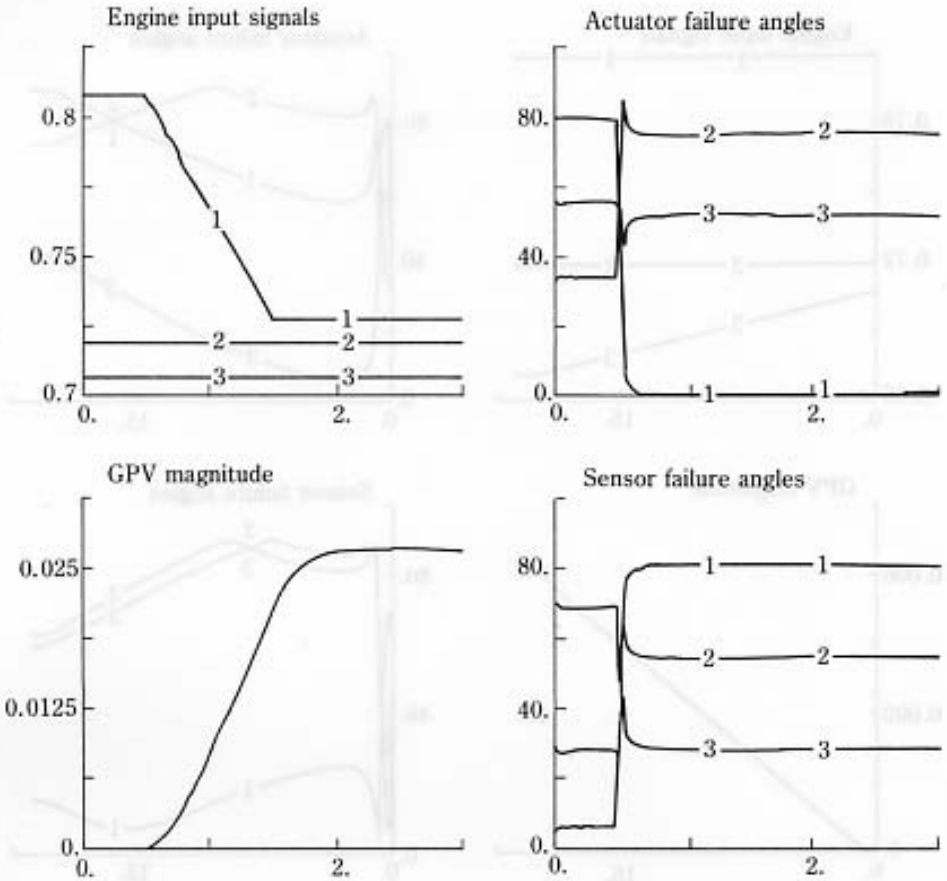

Fig. 6.1. Failure detection time-histories (−10[%] Bias, Actuator 1).

The isolation of failures in A8 may not be precluded by the problem discussed in the preceding paragraph. First, note that isolation for the other five input/output variables is so good that (for the cases shown in Tables 6.2 and 6.3) one may safely conclude that if the parity vector magnitude is large and the angle does not lie very close to one of the other 5 reference directions, then A8 (or some other component for which the algorithm was not designed) has failed. Alternatively, if the fault is small or occurs over a long period of time (many seconds), then it may be possible to take advantage of the fact that the parity vector/A8 failure reference direction angle is well behaved for small errors. Figure 6.2 is included to illustrate this: observe that fault isolation is quite definite for the first few seconds of the ramp failure.

Another simulation study was carried out to provide at least a preliminary assessment of the robustness of this FDI algorithm to linearization errors. As mentioned previously, the algorithm was designed based on a linearized model corresponding to operating point 9. As a test, we changed the nominal control

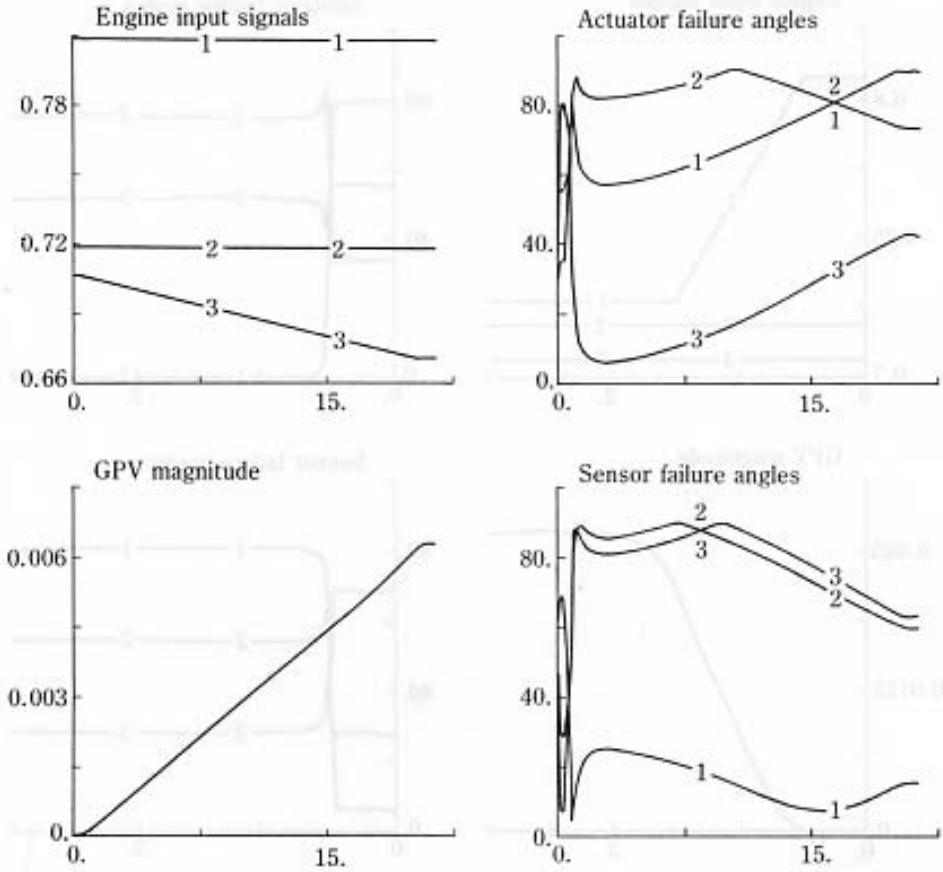

Fig. 6.2. Slow failure detection time-histories (Actuator 3).

Table 6.5. Steady-state angles between GPV and reference directions (transformed system, −5[%] ramp failure, operating point halfway between points 8 and 9)

Failure	GPV/reference directions (angles in degrees)						GPV magnitude
	Actuator			Sensor			
	WF36	STP48	A8	N2	N25	PS3	
NO FAILURE	16.9	87.9	43.7	70.1	70.5	45.1	6.2E-05
WF36	3.4	77.8	50.7	79.7	57.9	31.7	1.0E-02
STP48	70.4	4.7	75.7	87.8	23.7	54.6	1.4E-02
A8	45.4	75.5	7.2	37.7	75.0	67.8	7.5E-03
N2	81.8	87.6	30.3	0.2	74.8	74.7	2.3E-02
N25	54.7	27.5	80.5	74.7	0.1	32.6	3.8E-02
PS3	28.4	59.0	74.9	74.7	32.6	0.1	2.6E-02

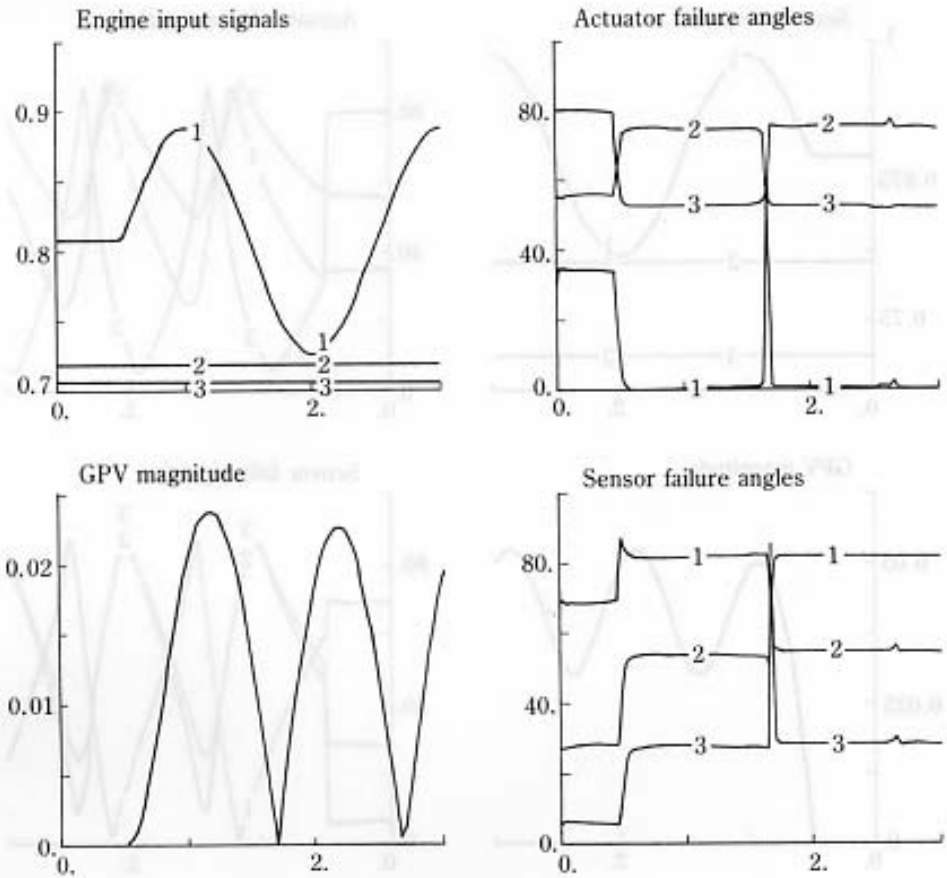

Fig. 6.3. Failure detection time-histories (−10[%] Sine, Actuator 1).

inputs to obtain an operating point of the nonlinear model that is half-way between operating points 8 and 9 and observed the performance of the scheme. The results shown in Table 6.5 demonstrate that (aside from the A8 problem mentioned above) the FDI algorithm continues to provide excellent results.

6.3.2. Sine error results A second investigation was performed, to demonstrate the significance of the assumption that the failures are of the bias type (which is central to the derivation of the steady-state GPV reference directions for sensors 1 and 2 used in the preceding FDI scheme), and to show that the more general algorithm which involves projecting the GPV into the appropriate subspaces (Sec. 6.1) can handle non-bias type sensor faults. To accomplish this, the errors were assumed to be 10[%] sinusoidal variations rather than biases, and both steady-state GPV direction and GPV projections onto reference planes were used for isolation.

The results for this test of the steady-state GPV direction algorithm are shown in Figs. 6.3 through 6.5; in summary:

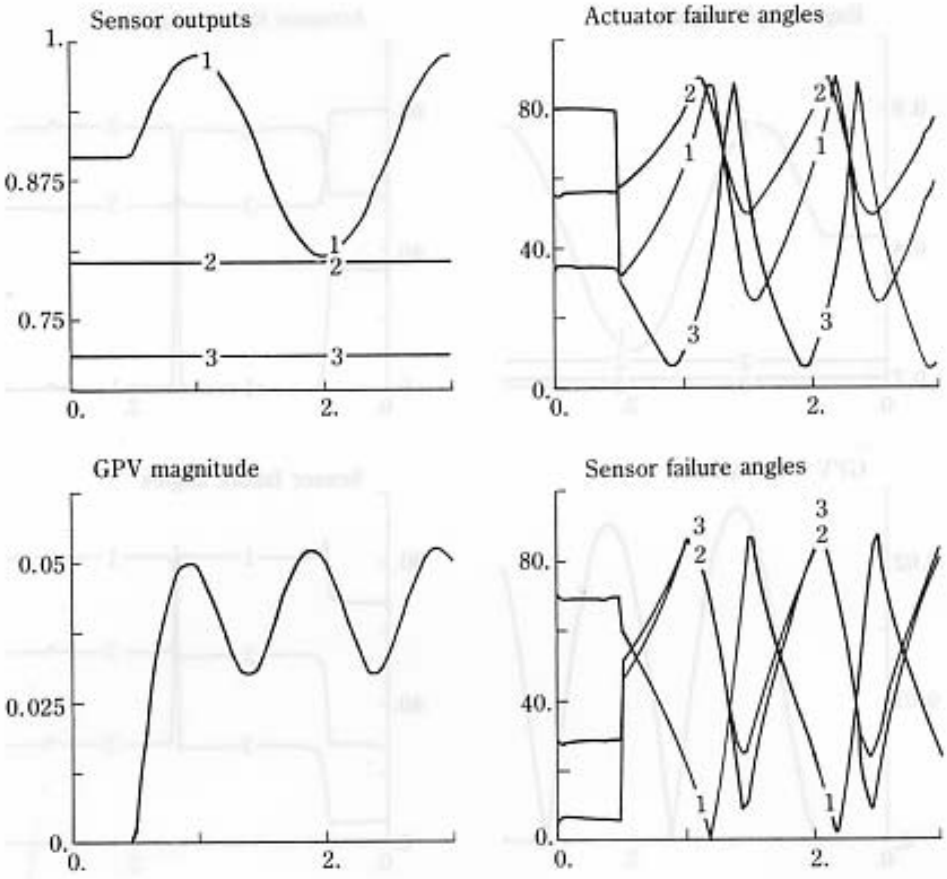

Fig. 6.4. Failure detection time-histories (−10[%] Sine, Sensor 1).

a. There is no problem detecting and isolating failures in the WF36 and STP48 actuators or in the PS3 sensor. There are only short-duration "blips" in the corresponding angle signal, which occur when the parity vector is small (at zero-crossings of the GPV); this is illustrated in Fig. 6.3 for WF36. The fact that the steady-state GPV direction could be used to isolate the PS3 sensor fault is a fortuitous result of the special form of $p_{s,3}$ (6.7).

b. N2 and N25 are the elements for which the steady-state GPV reference directions are not meaningful (see 6.6)). As shown in Fig. 6.4, a sinusoidal fault in sensor 1 results in a sensor angle that only momentarily dwells near 0° at points where the sensor output is most slowly changing (at the minimum and maximum point on the sine wave, i.e., at $t \cong 1.2$ and 2.2 seconds.

c. A8 produces poor results (Fig. 6.5), as expected, due to the nonlinearity of this actuator characteristic.

The ability to handle non-bias failures in the sensors can be regained by giving up the simplicity of the steady-state FDI algorithm. What is needed (see

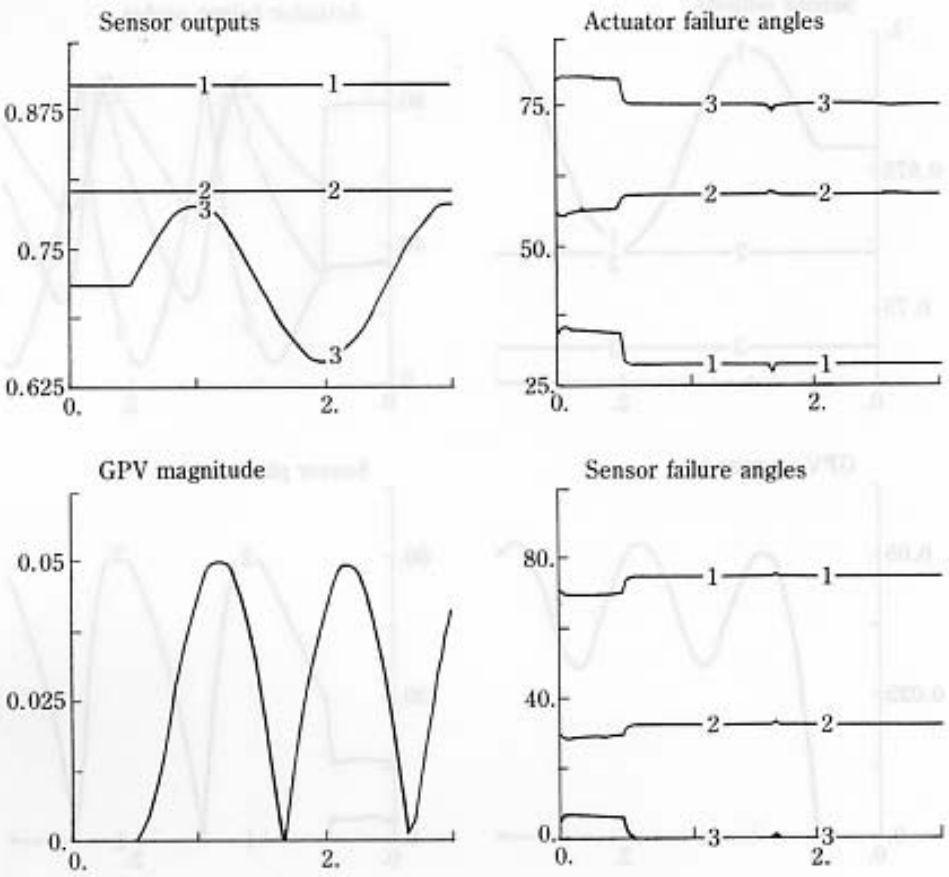

Fig. 6.5. Failure detection time-histories (−10[%] Sine, Actuator 3).

Sec. 6.1) is an implementation of the more general algorithm that projects the GPV into the appropriate subspace (plane) corresponding to each sensor failure. To do this, we look for GPV activity in the planes defined by the vectors $E_d{}^i$ and $B_d{}^i$ (see (6.6)); if the GPV is large and the activity is predominantly in the ith such plane, the ith sensor is declared to be failed. The results of applying this algorithm to a sinusoidal sensor 1 fault are portrayed in Fig. 6.6. Note that sensor plane angle 1 immediately goes to zero, while the rest of the angle signals are large, thus re-establishing unambiguous fault isolation. The same result was obtained for sensor 2.

In summary, the above results of applying the GPS approach to the GE-21 engine are very encouraging. Failure identification in sensors and actuators was conducted in a realistic nonlinear simulation environment, yielding generally good results. The only limitation appears to be due to unavoidable nonlinear effects in the engine response characteristics with respect to the A8 actuator.

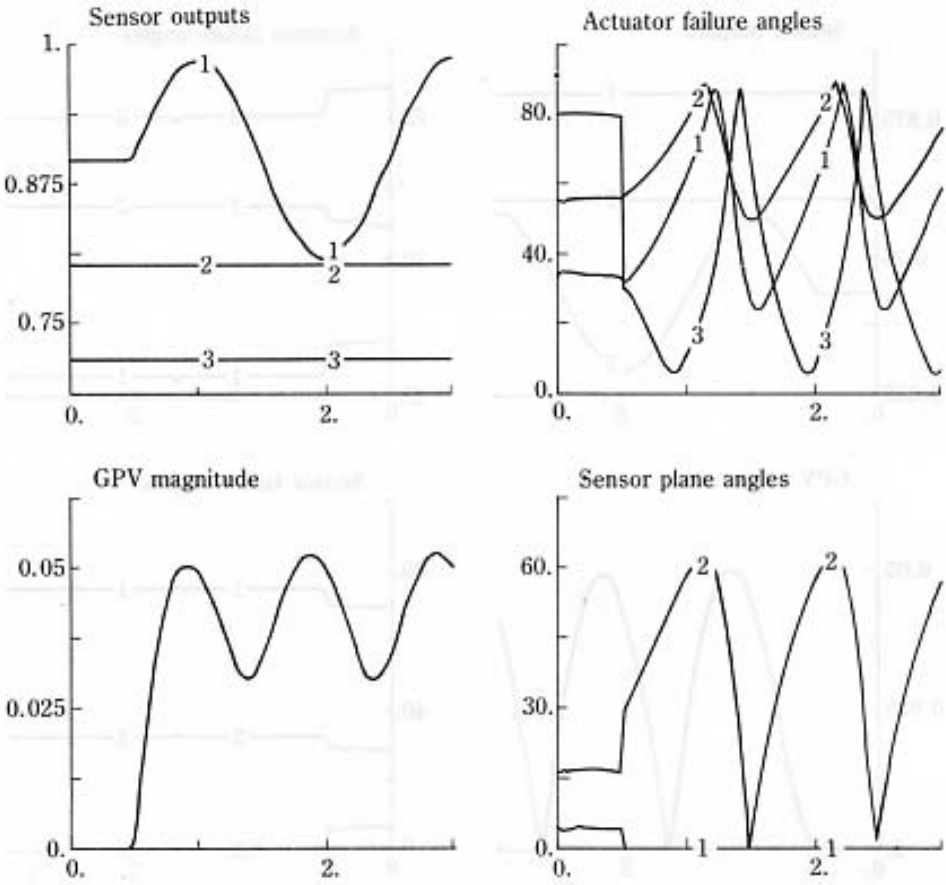

Fig. 6.6. Sensor failure detection time-histories—Non-steady-state algorithm (−10[%] Sine, Actuator 1).

7. Conclusions

In this paper, we have developed an elegant new formalism and several specific methods for fault detection and isolation (FDI) using the stable factorization framework. We have also discussed the use of various canonical forms and decoupling techniques to facilitate failure isolation. The most promising method, i.e., FDI based on the angle of the parity vector in the generalized parity space, was tested quite extensively for a GE-21 jet engine control system. This FDI scheme was able to identify failures in five of the six components very reliably and robustly when tested using the nonlinear simulation model. The A8 actuator faults were not so successfully handled by this FDI approach, because of the nonlinear effect of this input; despite this difficulty, however, it may be possible to deal with such failures involving highly nonlinear behavior, as our preliminary results show.

The results presented here could be extended in several ways: (i) the

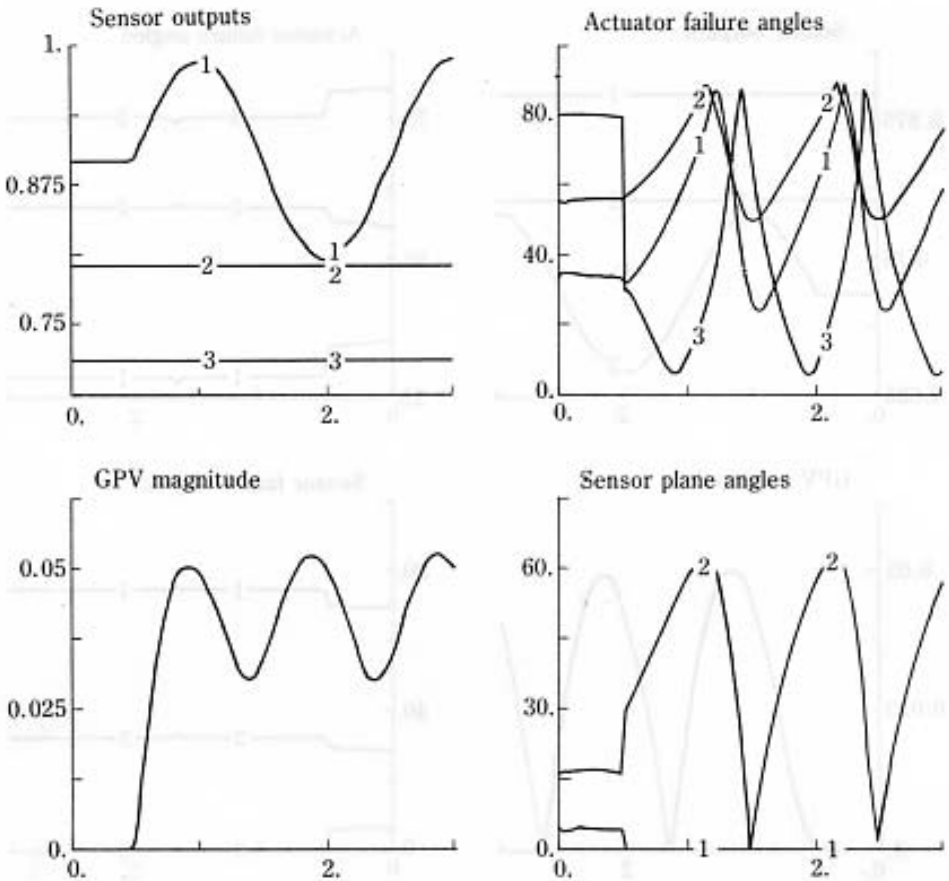

Fig. 6.6. Sensor failure detection time-histories—Non-steady-state algorithm (−10[%] Sine, Actuator 1).

7. Conclusions

In this paper, we have developed an elegant new formalism and several specific methods for fault detection and isolation (FDI) using the stable factorization framework. We have also discussed the use of various canonical forms and decoupling techniques to facilitate failure isolation. The most promising method, i.e., FDI based on the angle of the parity vector in the generalized parity space, was tested quite extensively for a GE-21 jet engine control system. This FDI scheme was able to identify failures in five of the six components very reliably and robustly when tested using the nonlinear simulation model. The A8 actuator faults were not so successfully handled by this FDI approach, because of the nonlinear effect of this input; despite this difficulty, however, it may be possible to deal with such failures involving highly nonlinear behavior, as our preliminary results show.

The results presented here could be extended in several ways: (i) the

generation of robust parity checks for FDI in uncertain dynamic systems, and (ii) extensions of the results to nonlinear and distributed parameter systems. Both of these extensions are possible, since theory is available for dealing with these issues in this context (Vidyasagar, 1985), and would be valuable in order to increase the power and applicability of this approach.

Acknowledgements

The first and third authors (NV, ECL) wish to acknowledge the financial support they received from the GE Corporate R & D Control Technology Branch during the period of this investigation.

References

Beard, R.V. (1971). Failure accommodation in linear systems through self organization. Rept. MVT-71-1, Man Vehicle Laboratory, MIT, Cambridge, MA, February.

Beattie, E.C. et al. (1981). Sensor failure detection system. Final Report, NASA-CR-165515, August.

Chow, E.Y. and A.S. Willsky. (1984). Analytical redundancy and the design of robust failure detection systems. *IEEE Trans. Automatic Control*, **AC-29**, 7, 603–614.

Clark, R.N., D.C. Fosth and V.M. Walton. (1975). Detecting instrument malfunctions in control systems. *IEEE Trans. Aero. and Elec. Systems*, **AES-11**, 4, 465–473.

Corley, R.C. and H.A. Spang. (1977). Failure detection and correction for turbofan engines. General Electric Co., Corporate Research and Development, Schenectady, N.Y., Report No.77CRD159.

Isermann, R. (1984). Process fault detection based on modelling and estimation—a survey. *Automatica*, **20**, 4, 387–404.

Jones, H.L. (1973). Failure detection in linear systems. Ph.D. Thesis, Dept. of Aero. and Astro., MIT, Cambridge, MA, September.

Kailath, T. (1980). *Linear Systems*. Prentice-Hall, Englewood Cliffs, N.J.

Kapasouris, P. (1984). Gain-scheduled multivariable control for the GE-21 turbofan engine using the LQR and LQR/LTR methodologies. Masters Thesis, LIDS, MIT, Cambridge, MA, May.

Kokawa, M. and S. Shingai (1982). Failure propagating simulation and nonfailure paths search in network systems. *Automatica*, **18**, 3, 335–341.

Lou, Xi-C., A.S. Willsky and G.C. Verghese. (1983). Failure detection with uncertain models. *Proc. 1983 American Control Conference*, 956–959, San Francisco, CA, June.

Lou, Xi-C., A.S. Willsky and G.C. Verghese (1986). Optimally robust redundancy relations for failure detection in uncertain systems. *Automatica*, **22**, 3, 333–344.

Mehra, R.K. and J. Peschon (1971). An innovations approach to fault detection in dynamic systems. *Automatica*, **7**, 5, 637–640.

Merrill, W., B. Lehtinen and J. Zeller (1984). The role of modern control theory in the design of controls for aircraft turbine engines. *J. Guidance and Control*, **7**, 6, 652–661.

Meserole, J.S. (1981). Detection filters for fault-tolerant control of turbofan engines. Ph.D. Thesis, Dept. of Aero. and Astro., MIT, Cambridge, MA, June.

Nett, C.N., C.A. Jacobson and M.J. Balas (1984). A connection between state space and doubly coprime fractional representations. *IEEE Trans. Automatic Control*, **AC-29**, 9, 831–832.

Potter, J.E. and M.C. Suman (1977). Threshold redundancy management with arrays of skewed instruments. AGARDOGRAPH-224, Integrity in Electronic Flight Control Systems, 15.11–15.25.

Teague, T.L. (1978). Diagnostic procedures from fault tree analysis. Masters Thesis, Dept. of Chem. Engg., Carnegie-Mellon Univ., Pittsburgh, PA.

Vidyasagar, M. (1985). *Control System Synthesis: A Factorization Approach*. MIT Press, Cambridge, MA.

Viswanadham, N. and D.P. Atherton (1976). A new approach for the design of noninteractive systems. *Int. J. Control*, **23**, 4, 535–540.

Weiss, J.L., A.S. Willsky, K.R. Pattipati and J.S. Eterno (1985). Application of FDI metrics to detection and isolation of sensor failures in turbine engines. Technical Paper TP-222 ALPHATECH, March. *Proc. 1985 American Control Conference*, 1114–1120, Boston, MA, June.

Willsky, A.S. (1976). A survey of design methods for failure detection in dynamic systems. *Automatica*, **12**, 6, 601–611.

Willsky, A.S. (1980). Failure detection in dynamic systems. AGARD Lecture Series Number 109 on Fault Tolerance Design and Redundancy Management Techniques, October.

Willsky, A.S. and H.L. Jones (1976). A generalized likelihood ratio approach to detection and estimation of jumps in linear systems. *IEEE Trans. Automatic Control*, **AC-21**, 1, 108–112.

Wolovich, W.A. (1974). *Linear Multivariable Systems*. Springer, N.Y.